

# Synthesis, characterization and biological evaluation of hexagonal wurtzite structured ZnO nanoparticle from Zn (II)-Schiff base complex

Ikechukwu P. Ejidike<sup>1\*</sup>, Mercy O. Bamigboye<sup>2</sup>, Racheal U. Ijimdiya<sup>1</sup>, Dories O. Seyinde<sup>1</sup>, Oluwatoyin O. Ojo<sup>1</sup>

## Affiliation

<sup>1</sup>Department of Chemical Sciences, Faculty of Science and Science Education, Anchor University, Lagos, Nigeria

<sup>2</sup>Department of Industrial Chemistry, Faculty of Physical Sciences, University of Ilorin, Ilorin, Nigeria

## \*For Correspondence

**Email:**iejidike@aul.edu.ng; **ORCID:**<https://orcid.org/0000-0002-3643-0198>

## Abstract

Studies on transitional metal compounds of Schiff base ligands have been of great significance due to their spectral properties and wide applications. Tetradentate Schiff base-Zn (II) complex was prepared and used as a precursor for the synthesis of Zinc oxide (ZnO) nanoparticles through a one-step calcination process at a different temperature: 250-350 °C. The influence of temperature on the antioxidant activities of synthesized nanoparticles was investigated. The precursor (zinc complexes) was characterized by melting point, thermogravimetric analysis, UV-Vis, FT-IR spectroscopy. elemental analysis, and thermogravimetric analysis (TGA) of tridentate Schiff base was synthesized and characterized using The structural studies of synthesized metal oxides were carried out with powder X-ray diffraction (PXRD), transmission electron microscopy (TEM), FTIR, and UV-visible. The energy band gap of the nanoparticles was 3.15 eV for ZnO@250, 3.31 eV for ZnO@300, while ZnO@350 was found as 3.17 eV and 3.56 eV. The average sizes of the ZnO nanoparticles were found to be around 25 nm. The antioxidant activities of the product were investigated through scavenging activity on DPPH. The obtained IC<sub>50</sub> value of the DPPH activity for the product @ 350 °C (IC<sub>50</sub> = 4.09 ± 0.32µM) was higher than other nanoparticles.

**Keywords:** Schiff base, Zinc Oxide, DPPH, Metal complexes, Antioxidant, Nanoparticles.

## Introduction

Metal complexes containing Schiff base are of interest because of their electronic properties that can be modified by suitable functionalization with amine and cyclic substituents (Ejidike and Ajibade, 2017; Ejidike, 2018). Also, tetradentate Schiff base complexes have shown high stability when coordinated to metal ion using the N<sub>2</sub>O<sub>2</sub> donor atoms (Alias *et al.*, 2014, Emara *et al.*, 2014; Ejidike and Ajibade, 2017). There have been current advances primarily with the capability to prepare highly ordered nanoparticles of assorted shapes and sizes, in the field of nanotechnology, and this has led to the development to new materials possessing various biological activities (Meruvu *et al.*, 2011; Gunalan *et al.*, 2012; Navale *et al.*, 2015; Stan *et al.*, 2016).

Metal oxide nanoparticles can be obtained by various methods depending on the chemical and physical techniques employed. Metal oxide nanoparticles and composite materials are widely applied in the field of research and development and diverse applications in industries including surface coatings, bioengineering, bio-diagnostics, optoelectronics, and agriculture (Navale *et al.*, 2015; Malathy *et al.*, 2017). Zinc oxide nanoparticles (ZnO NPs) have received considerable attention due to their unique antibacterial, antifungal, and UV filtering properties, high catalytic and photochemical activity (Stan *et al.*, 2016). Among the metal oxide nanoparticles, zinc oxide is interesting because it has vast applications in various areas such as optical, piezoelectric, magnetic, and gas sensing (Navale *et al.*, 2015; Stan *et al.*, 2016; Xaba *et al.*, 2016). Besides these properties, ZnO nanostructure exhibits high catalytic efficiency, strong adsorption ability and are used more and more frequently in the manufacture of sunscreens (Meruvu *et al.*, 2011; Kumar *et al.*, 2014; Navale *et al.*, 2015), ceramics and rubber processing, wastewater treatment, and as a fungicide (Stan *et al.*, 2016; Navale *et al.*, 2015). Nanostructures based on zinc oxide are predominantly interesting because of their n-type conductivity with a wide band gap of 3.3 eV, making ZnO materials more suitable for modern technologies (Kalpanadevi *et al.*, 2013; Kulkarni and Shirsat, 2015; Xaba *et al.*, 2016). The significance of ZnO NPs in various areas has led to its global interest in studying their antifungal, antibacterial, antioxidant, and anticancer activity. Literatures on the biological activities actions of ZnONPs have stimulated a considerable range of antimicrobial and toxicity applications. ZnO NPs are used as antibacterial agents owing to the unique properties and excellent stability with long life as compared to organic-based disinfectants (Kumar *et al.*, 2014; Stan *et al.*, 2016). The large surface-area-to-volume ratio allows their use as novel biological agents. This unique property has also predicted to enhance ZnO NPs applications in several areas, such as in catalysis and biomedicine, food industry (Meruvu *et al.*, 2011; Kumar *et al.*, 2014; Stan *et al.*, 2016)

Reactive oxygen species (ROS) or free radicals are products of the in vivo physiological and biochemical processes in the living cells (Ejidike and Ajibade, 2017) that could cause lipid peroxidation and may lead to diseases such as cancer, cardiovascular diseases, immunodeficiency, liver injury and other infections (Ejidike and Ajibade, 2015; 2017). To safeguard the human body against cell damage by oxidative species, antioxidant is of paramount importance (Ejidike and Ajibade, 2015). Due to many biological processes taking place at the nanoscale level, there is the potential that engineered nanomaterials may interact with biomolecules and cellular processes; hence, ZnO nanoparticles are believed to be safe, non-toxic, and biocompatible. Based on the above facts in the present work, we report the synthesis and characterization of Zn(II) Schiff base complexes and its ZnO nanoparticles. Also, reported are the antiradical activities of the synthesized nanomaterials.

## **Experimental Materials**

All chemicals and solvents were of analytical grade and used as obtained without any further purification. Ethylenediamine and the zinc chloride acetate were purchased from Merck, South Africa; 2',4'-dihydroxyacetophenone, Ascorbic acid, gallic acid, and 2-hydroxybenzaldehyde were purchased from Sigma-Aldrich (Johannesburg, South Africa); 1,1-diphenyl-2-picrylhydrazyl (DPPH) was purchased from Sigma Chemical Co., USA. Perkin Elmer FT-IR spectrometer (Spectrum 2000) in the range 4000–400  $\text{cm}^{-1}$  was used for IR spectra data collection. A freshly prepared 10<sup>-3</sup> M DMF solution with PC 7000 conductivity cell was used for the conductivity

measurements. The analyses of carbon, hydrogen, and nitrogen were determined on a Perkin Elmer elemental analyzer (2400 Series). Electronic spectra were recorded on a model T80+ UV-Vis spectrometer in the range 200–800 nm. Thermal Decomposition of the Complexes were recorded on the Thermogravimetric analyzer: TGA 4000 System. SMP 10 Melting Point Apparatus was used for the melting points analysis. Transmission electron microscopy (TEM) studies were performed using a JEOL JEM-2100F TEM operated at an accelerating voltage of 200 kV.

### Preparation of Schiff base ligand

The ligand (L) was prepared according to the previous report (Ejidike, 2018). 1,2-ethylenediamine (0.015 mol) dissolved in 30 ml of ethanol was slowly added to an ethanol solution (30 ml) containing 2-hydroxybenzaldehyde (0.015 mol), followed by the slow addition of 2',4'-dihydroxyacetophenone (0.015 mol) dissolved in 30 ml ethanol. The resulting coloured mixture was refluxed with stirring for 4.5 h. It was cooled and the resulting precipitate was filtered, washed with ethanol, and then recrystallization in ethanol (Yield = 91.20 %).

### Preparation of the Precursor [Zn-L] complex

In a typical experiment, the metal complex was obtained by adding 0.01 mol of  $\text{Zn}(\text{acet})_2 \cdot 2\text{H}_2\text{O}$  dissolved in 30 ml of ethanol, into a warm ethanolic solution (40 ml) of (0.01 mol) ligand (L) with constant stirring. The resulting solution was then refluxed for 3 h and allowed to cool to room temperature. The solid formed was filtered, and the precipitate was carefully washed with cold ethanol and diethyl ether, dried over dry calcium chloride, and characterized (Scheme 1).

**Ligand ( $\text{C}_{17}\text{H}_{18}\text{N}_2\text{O}_3$ ):** The ligand was obtained as a yellowish solid. Percentage yield (%): 91.20. Decomp. Temp.: 198-199 °C. Formula weight: 298.34 g. Anal for  $\text{C}_{17}\text{H}_{18}\text{N}_2\text{O}_3$  calcd.: C, 68.44; H, 6.08; N, 9.39 %. Found: C, 67.91; H, 6.74 N, 8.98 %. FT-IR spectral bands ( $\text{cm}^{-1}$ ):  $\nu(\text{OH})$ , 3365;  $\nu(\text{C}=\text{N})$ , 1582. UV-vis ( $\lambda_{\text{max}}$ , nm): 295, 320, 400.

**Zn( $\text{C}_{17}\text{H}_{16}\text{N}_2\text{O}_3$ ) complex:** The complex was obtained as a lemon-yellow solid. Percentage yield (%): 73.28. Decomp. Temp.: 225-226 °C. Formula weight: 361.73 g. Anal for  $\text{C}_{17}\text{H}_{16}\text{ZnN}_2\text{O}_3$  calcd.: C, 56.45; H, 4.46; N, 7.74 %. Found: C, 57.01; H, 5.04 N, 7.49 %. Conductivity ( $\mu\text{S}/\text{cm}$ ): 14.15. FT-IR spectral bands ( $\text{cm}^{-1}$ ):  $\nu(\text{OH})$ , 3399;  $\nu(\text{C}=\text{N})$ , 1589;  $\nu(\text{M}-\text{O})$ , 626;  $\nu(\text{M}-\text{N})$ , 437. UV-vis ( $\lambda_{\text{max}}$ , nm): 295, 325, 410.

### Preparation of Zinc Oxide Nanoparticles

Zinc oxide nanoparticles were obtained by the Calcination method (Malathy *et al.*, 2017) of the precursor. In this method, the dried precursor (Zinc Schiff base complex) was transferred to a silica crucible and heated in an electric furnace at various temperatures such as 250 °C, 300 °C and 350 °C (Table 1). in an ordinary atmosphere for about 1 h. The precursor started decomposing gradually, and the total decomposition of the precursor complex led to the formation of the ZnO nanoparticles, which are quenched to room temperature, and stored in a desiccator. The pure ZnO NPs obtained were characterized by spectral studies (Scheme 2).

**Table 1: Codes used for the samples descriptions**

Codes	Description
ZnO@250	ZnO nanoparticles prepared at 250 °C
ZnO@300	ZnO nanoparticles prepared at 300 °C

## Biological Evaluations

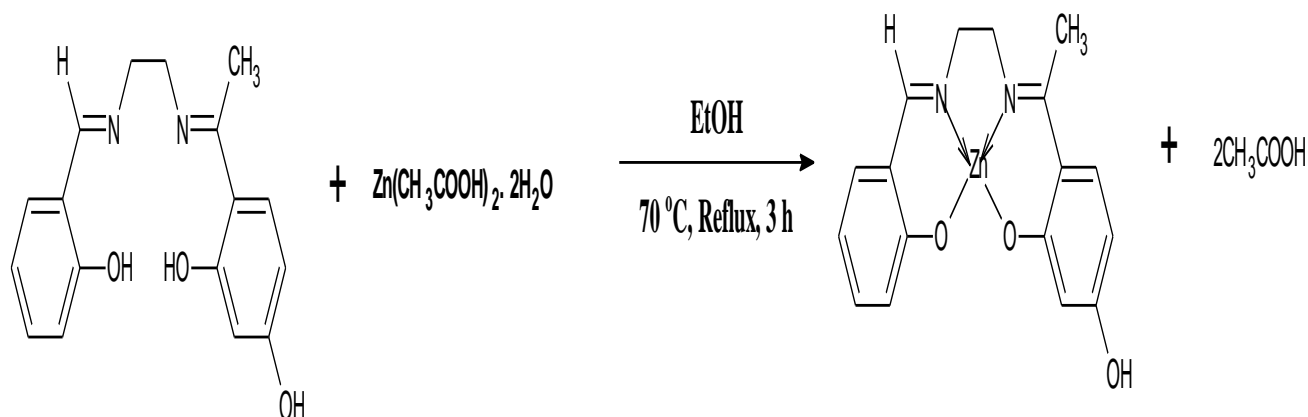
### 2,2-Diphenyl-1-picrylhydrazyl (DPPH) Radical Scavenging Activity

DPPH (1,1-diphenyl-2-picryl-hydrazyl) radical scavenging activity evaluation is a standard assay used in antioxidant activity studies. The antioxidant activity of the ZnO nanoparticles was studied spectrophotometrically by the DPPH method (Ejidike and Ajibade, 2017). It is a rapid technique for screening the radical scavenging activity of synthesized compounds (Ejidike, 2018). The radical scavenging properties of the synthesized zinc oxide nanoparticles with DPPH radical were assessed at different concentrations of the test compounds in DMF solutions (1 mL), added to 1.0 mL of 0.4 mM DPPH in methanol and mixed thoroughly by the vortex. The mixtures were allowed to incubate at room temperature in the dark for 30 min, after which the scavenging power of the test samples was measured concerning a decrease in the absorbance of DPPH at 517 nm. All tests analysis was performed in triplicates, to obtain the mean  $\pm$  SD.

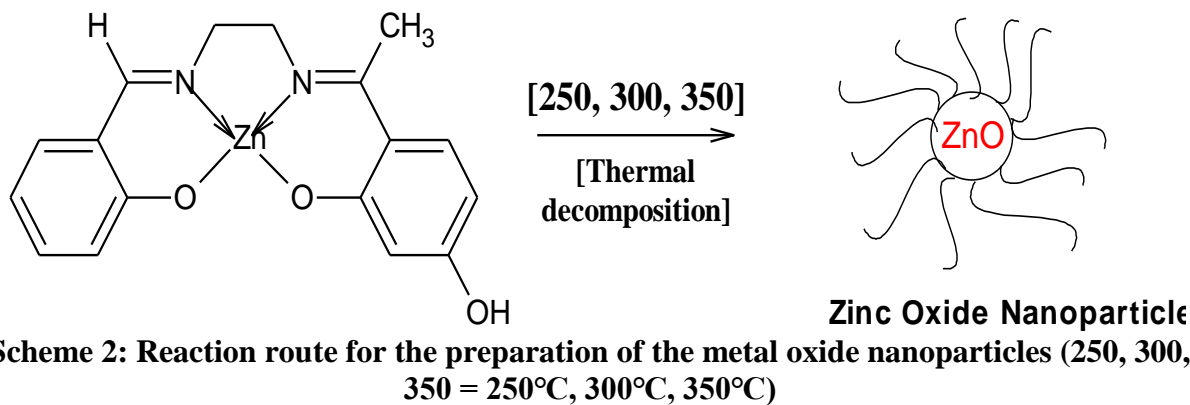
$$\% \text{ scavenging activity} = \frac{\text{Absorbance of control} - \text{Absorbance of sample}}{\text{Absorbance of control}} \times 100 \quad (1)$$

## Results and Discussion

The metal complex was obtained by the reaction of zinc acetate in methanol with the ligand in a 1:1 mole ratio. The complex analytical data disclose metal: ligand molar ratio (1:1) for the system (Scheme 1). The complex was soluble in DMF, DMSO, and insoluble in other organic mediums, with molar conductivity measured in DMF solution indicating a non-electrolyte character.



**Scheme 1: Reaction route for the preparation of the metal complexes**



### FTIR Spectra

A band around  $3365\text{ cm}^{-1}$  is assigned to  $\nu(\text{OH})$  stretching vibrations of the free Schiff ligand. In the complex spectra, this band shifted to  $\sim 3399\text{ cm}^{-1}$  owing to the  $\nu(\text{OH})$  stretching of the moisture content within the complex (Alias *et al.*, 2014, Emara *et al.*, 2014; Ejidike, 2018). The intense band observed at  $1582\text{ cm}^{-1}$  in the free ligand assigned azomethine  $\nu(\text{C}=\text{N})$  stretching vibration (Ejidike and Ajibade, 2017) was shifted toward higher wave number in the metal complex spectra (Figure 1). This shifting towards higher wave number around  $1589\text{ cm}^{-1}$  regions is due to the coordination of the azomethine ( $>\text{C}=\text{N}$ ) nitrogen atoms with the central metal ion (Malathy *et al.*, 2017; Ejidike, 2018). The stretching vibration of the phenolic  $\nu(\text{C}-\text{O})$  observed at  $1240$ , and  $1170\text{ cm}^{-1}$  in the free Schiff base (Kumar *et al.*, 2014; Ejidike, 2018) undergo a hypochromic shift to  $1243$  and  $1173\text{ cm}^{-1}$  regions in the zinc complex upon complexation. This shift further confirms the coordination of the phenolic oxygen leading to the formation of the  $\text{C}-\text{O}-\text{Zn}$  bond (Ejidike and Ajibade, 2017). New bands observed around region  $626\text{ cm}^{-1}$  in the complexes are assigned to  $\nu(\text{M}-\text{O})$  stretching vibrations while those in the region  $437\text{ cm}^{-1}$  are due to  $\nu(\text{M}-\text{N})$  (Ejidike and Ajibade, 2017; Malathy *et al.*, 2017).

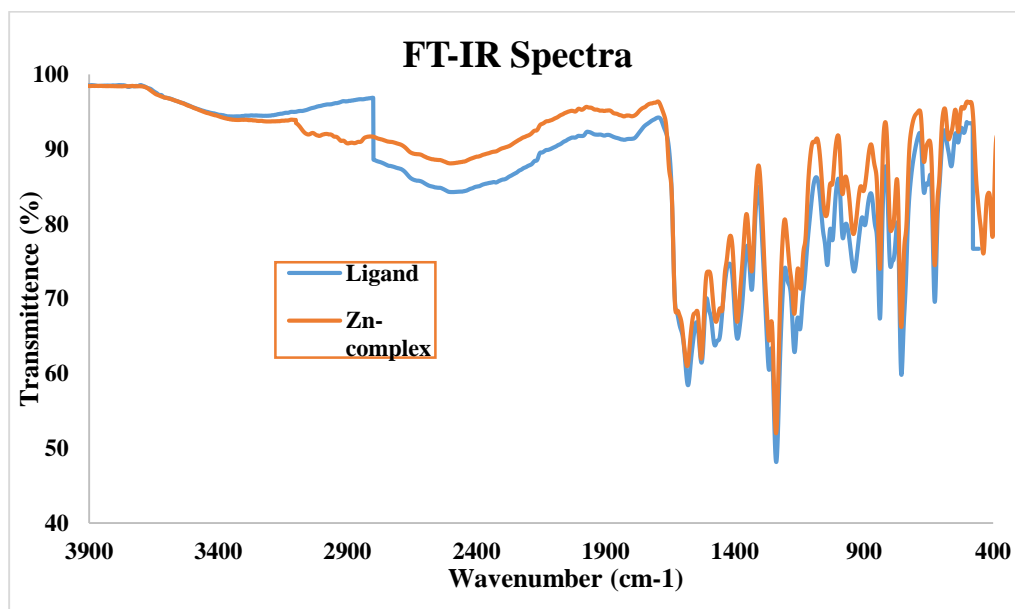


**Figure 1: FT-IR for Ligand (L) and complex (Zn-L)**

### UV-vis Spectra

The UV-visible spectra of the free ligand (L) and the metal complex [Zn-L] are shown in Figure 2. The ligand (L) spectra show bands in the region 295 and 320 nm which is attributed to  $\pi-\pi^*$  for the aromatic system, while the third band is due to  $n-\pi^*$  transition within  $>C=N$  group. The  $\pi-\pi^*$  transition was shifted to a corresponding wavelength 295 and 325 nm upon the formation of the zinc complex (Figure 2). The wavelength observed at 400 nm in the UV – Vis spectra of the ligands (L) corresponding to the  $n-\pi^*$  transition was shifted to 410 nm in the complex upon complexation, this is an indication of the coordination of ligand to zinc ion (Alias *et al.*, 2014, Ejidike, 2018). The Zn(II) complex, showed an absorption band at 410 nm is due to the LMCT/ MLCT transitions of zinc complex in a tetrahedral geometry, as no d-d electronic transition is expected (Malathy *et al.*, 2017; Ejidike, 2018).

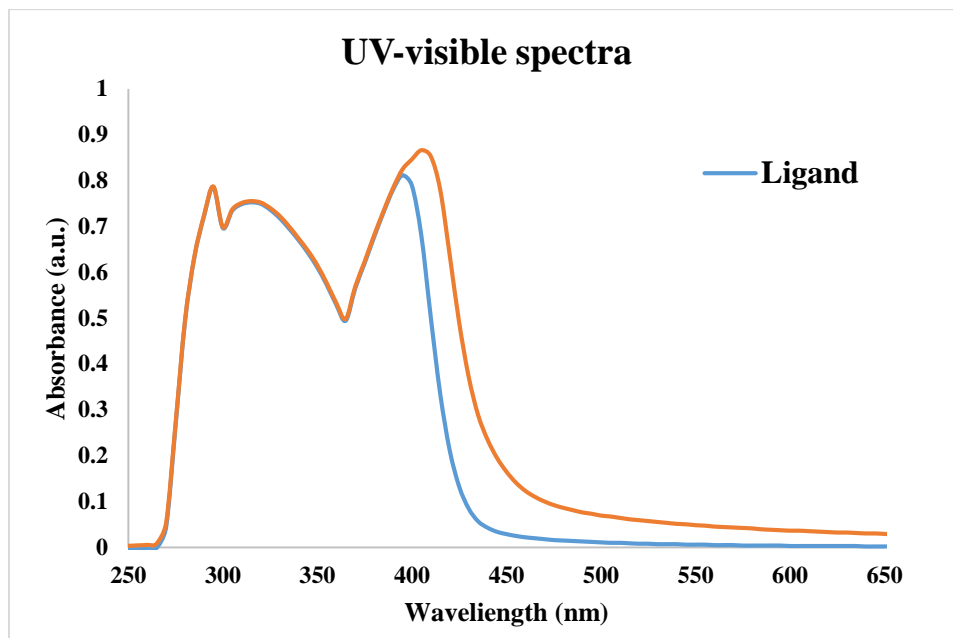


**Figure 2: UV-Vis for ligand and Zn (II) complex**

### Thermogravimetric analysis (TGA)

Thermogravimetric and derivative thermogravimetric analysis (TGA/DTA) of the synthesized Zinc-Schiff base complex was measured under a nitrogen atmosphere at a heating rate of  $10\text{ }^{\circ}\text{C min}^{-1}$  from  $20\text{ }^{\circ}\text{C}$  to  $900\text{ }^{\circ}\text{C}$ . TG/DTG results were plotted as % weight loss against temperature; provides insight into nature, properties of different molecules, and the residues obtained after thermal decomposition. The loss of lattice water and part of the anchoring ligand in the zinc-complex occurs between the temperature ranges of  $134 - 255\text{ }^{\circ}\text{C}$ . Above this temperature, as displayed in Figure 3, it revealed a strong endothermic peak in the range of  $297 - 396\text{ }^{\circ}\text{C}$  for the as-synthesized complex. The differential thermogravimetric curve illustrates that most of the weight loss occurred at about  $319\text{ }^{\circ}\text{C}$ . It exhibited a sharp decomposition with a mass loss of 55.02 %, which is assignable for the loss of the ligand moiety, which gives zinc oxide as the final residue (Kalpanadevi *et al.*, 2013; Malathy *et al.*, 2017; Ejidike, 2018).

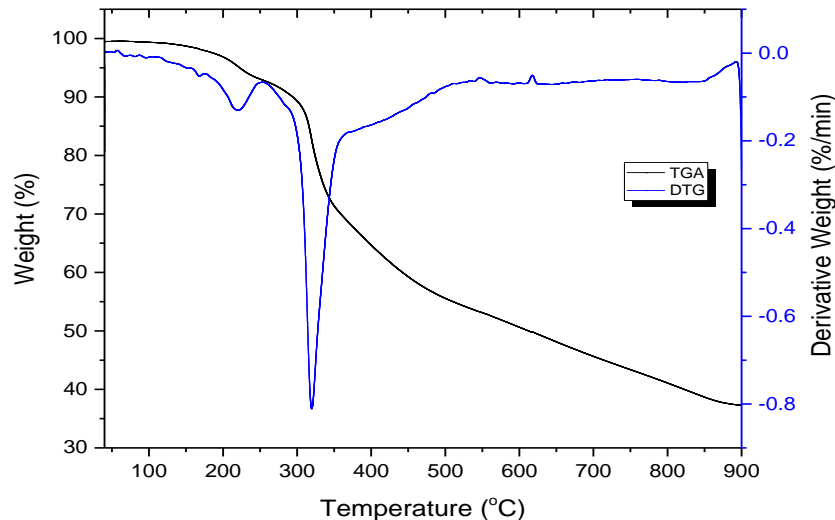


**Figure 3: TG and DTG curves of Zn (II)-complex**

### Characterization of Zinc Oxide Nanoparticles

#### FTIR Spectra for ZnO

The FTIR spectra of the ZnO Np's synthesized from the complex, shows  $\nu(\text{Zn-O})$  vibrations at  $761\text{ cm}^{-1}$ . The presence of the O-H group represents the presence of water molecules on the surface of ZnO nanoparticles (Kalpanadevi *et al.*, 2013; Stan *et al.*, 2016; Ejidike, 2018).

#### Optical Properties of Zinc Oxide Nanoparticles

The absorptions spectra of the zinc oxide nanoparticles are presented in Figure 4a. UV-Visible spectra analysis has served as a useful technique for the characterization of semiconductor nanoparticles, which exhibit quantum size effect. The UV-Vis absorption spectra (Figure 4) showed that the absorption peaks at 382 nm for ZnO@250, 380 nm for ZnO@300, and 306 and 336 nm for ZnO@350 of the analysed ZnO particles, which are relatively blue-shifted of the bulk ZnO materials (Kalpanadevi *et al.*, 2013; Xaba *et al.*, 2016; Gharibshahi *et al.*, 2017). The band gap of the ZnO nanoparticles were calculated by extrapolating the curve drawn between the square of  $(\alpha h\nu)$  versus  $(h\nu)$  as displayed in Figure 4b. Where  $\nu$  is the frequency and  $\alpha$  is the optical absorption coefficient. Therefore, the band gap energy was obtained by extrapolating the curve and found to be approximately 3.15 eV for ZnO@250, 3.31 eV for ZnO@300, while ZnO@350 was found as 3.17 eV and 3.56 eV. The blue shifts of the ZnO nanoparticles are indicative of quantum confinements of the nanoparticles (Kulkarni and Shirsat, 2015).

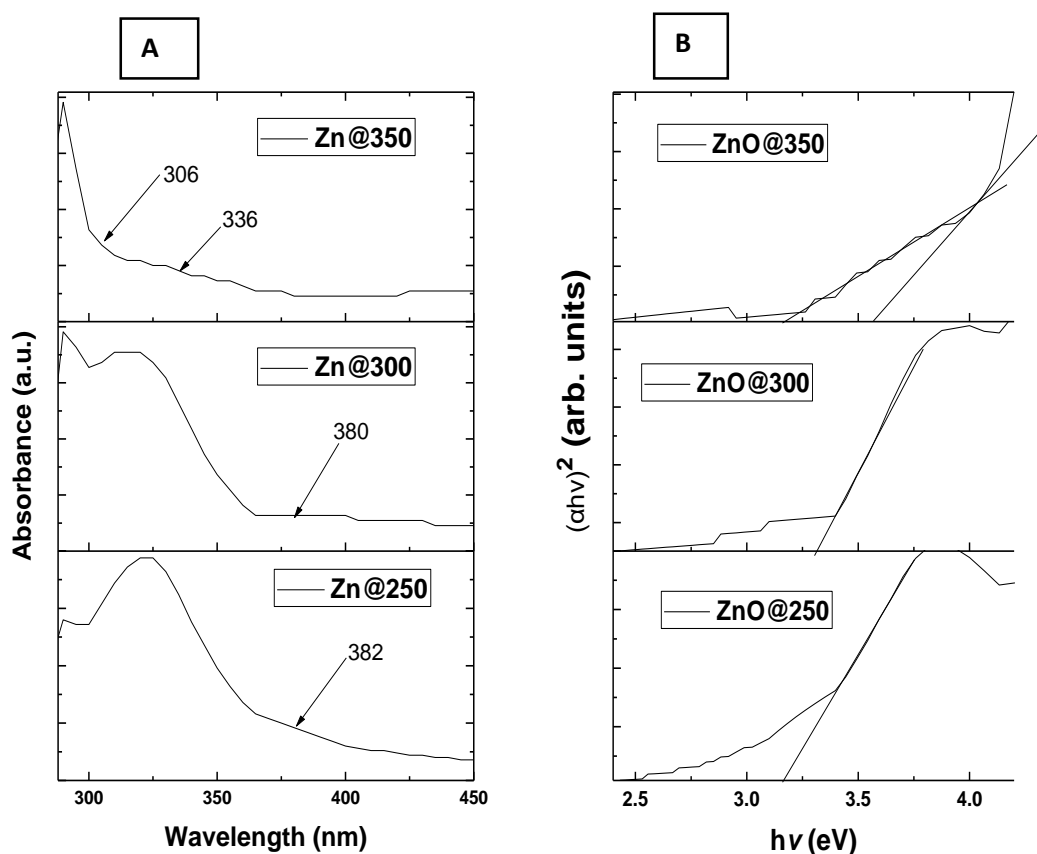


**Figure 4: (A) UV-Vis spectra of the nanoparticles; (B) Tauc Plot from UV-Vis spectra for band gap determination of as-synthesized ZnO nanoparticles**

### X-ray diffraction studies of ZnO nanoparticles

The X-ray diffraction peaks of ZnO nanoparticles are shown in Figure 5. The positions of XRD peaks observed in the patterns of the synthesized ZnO nanoparticles corresponds to the planes (100), (002), (101), (102), (110), (103), (202), (112), and (201) showing a good agreement with those of the hexagonal wurtzite structure for bulk ZnO with lattice constants of  $a = 0.3249$  nm and  $c = 0.5208$  nm (JCPDS card No. 36-1451, P63mc) (Navale *et al.*, 2015; Kulkarni and Shirsat, 2015). The average crystallite size ( $D$ ) of the Zn-NPs is calculated after appropriate background corrections from X-ray line broadening of the diffraction peaks using Debye Scherrer's formula

$$D = 0.9\lambda / \beta \cos\theta \quad (2)$$

where  $\lambda$  is the wavelength of X-ray used (1.5405 Å),  $\beta$  is the angular peak width at half maximum in radians and  $\theta$  is the Bragg's diffraction angle. The average particle sizes are calculated to be around 25 nm. The observed diffraction peaks were broad around their bases, signifying that the ZnO nanoparticles are in a nanosized regime (Kulkarni and Shirsat, 2015; Xaba *et al.*, 2016).

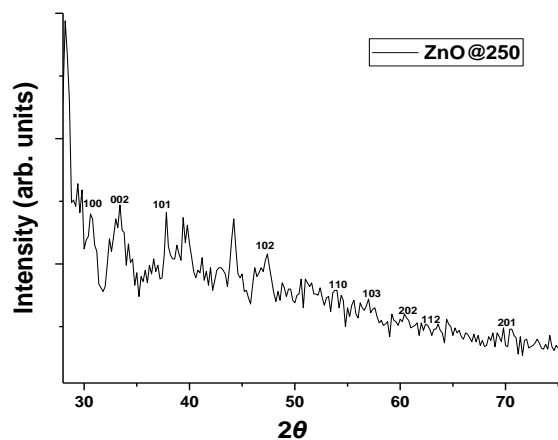


**Figure 5: XRD diffraction pattern of ZnO nanoparticles**

### Transmission Electron Microscopy (TEM) Studies

The morphological characteristics of the zinc oxide nanoparticles revealed by TEM images are shown in Figure 6. The TEM images of ZnO NPs demonstrate the presence of nanocrystalline particles and aggregation with different shapes and sizes depending on the temperature rate used for nanoparticle synthesis (Kalpanadevi *et al.*, 2013; Xaba *et al.*, 2016; Gharibshahi *et al.*, 2017). ZnO NPs were prepared by decomposition method, possess slightly spherical, and are loosely distributed with an average particle size in the range of 23 nm and 30 nm. The average particle size of ZnO nanoparticles obtained from TEM image analysis is consistent with the average crystallite size as assessed by XRD analysis.

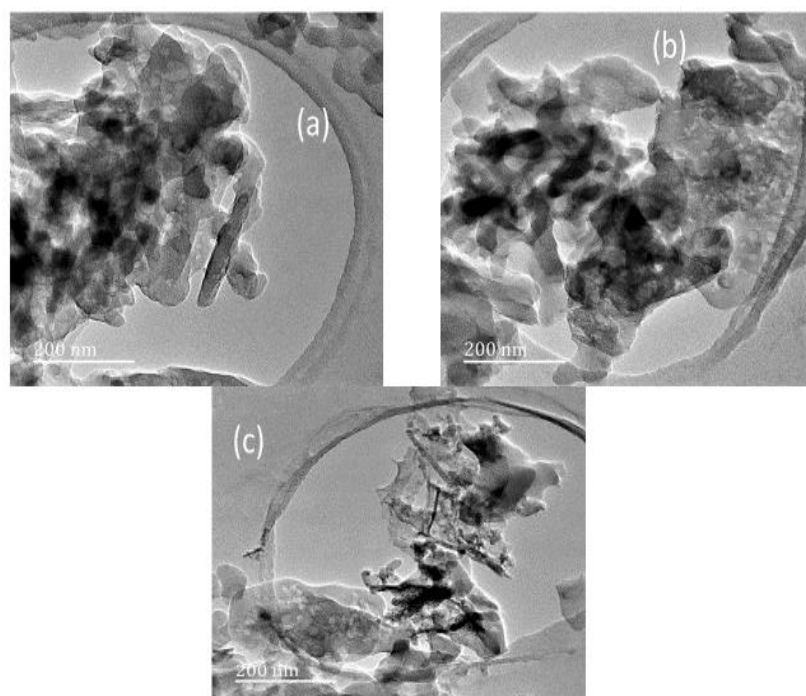


**Figure 6: TEM micrographs of ZnO NPs: (a) ZnO@250, (b) ZnO@300, (c) ZnO@350**

## Biological evaluation of ZnO nanoparticle

The antioxidant activity of the ZnO nanoparticles was studied spectrophotometrically using the DPPH method alongside the standards agents- gallic acid and ascorbic acid, as displayed in Figure 7. (Ejidike and Ajibade, 2017). Radical scavenging activity of nanoparticles, as well as the standards, exhibited appreciable activities. However, the activities of standard drugs (gallic acid and ascorbic acid) possess higher antioxidant potential ( $IC_{50}$ ) than ZnO nanoparticles. The DPPH radical scavenging activity decreased as follows: Ascorbic acid > Gallic acid > ZnO@350 > ZnO@250 > ZnO@300. The scavenging potentials of the ZnO nanoparticles could be ascribed to electron density transfer located at oxygen to the odd electron located at nitrogen atom in DPPH (Stan *et al.*, 2016). The scavenging potentials of the nanoparticles are associated with the presence of negatively charged active compounds such as  $COO^-$  and  $O^-$  of the ligand and positively charged nanoparticles ( $ZnO = Zn^{2+} + O^{2-}$ ) that exerted electrostatic attraction required for the breaking of free radical chains (Kumar *et al.*, 2014; Stan *et al.*, 2016; Ejidike, 2018). The differences in the scavenging activity of the synthesized ZnO using the ONNO Schiff base zinc complex could be related to the fact that the nanoparticles possess different sizes and specific surfaces according to the different temperatures used in the synthesis process. The ZnO@350 samples which have the smallest nanoparticle size showed the highest DPPH scavenging activity amongst the nanoparticles.

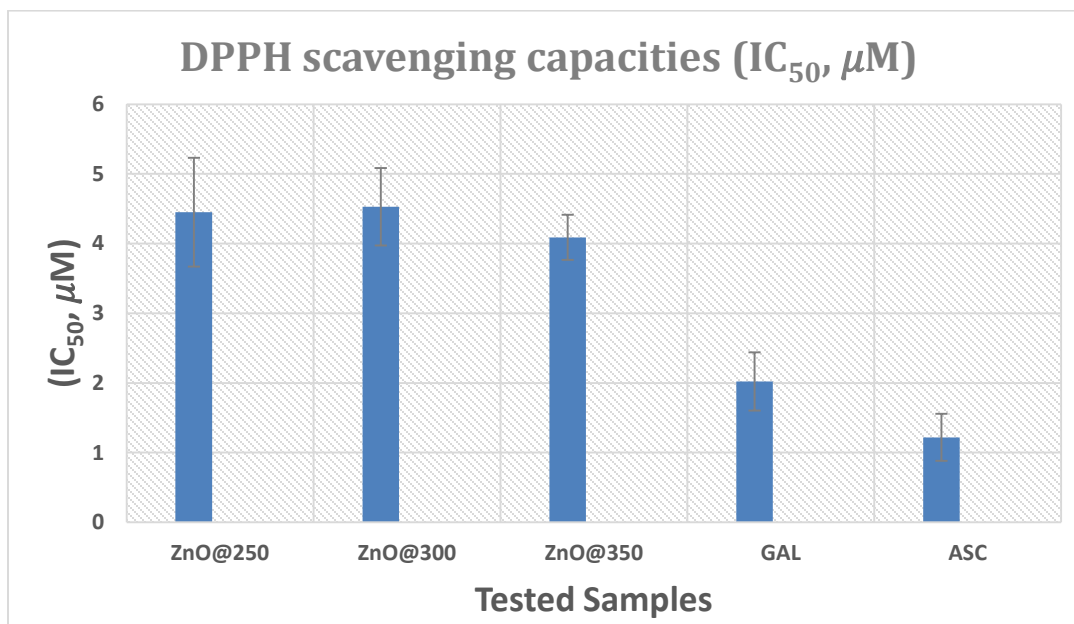


**Figure 7: DPPH scavenging capacities ( $IC_{50}$ ,  $\mu M$ ); ASC = Ascorbic acid and GAL = Gallic acid**

## Conclusion

The main goal of the present work is to synthesize Zinc Oxide nanoparticles from the Schiff base complex and their application as antiradical agents. Zinc ion to ligand binding was confirmed by spectral analyses. Ligand-Zn complex was observed to possess tetrahedral geometry. The thermal stability of the complexes was obtained by TGA studies. Formation of the ZnO nanoparticles synthesized from Zn(II) complexes were confirmed by FT-IR, UV-Vis, XRD, and TEM spectra. The energy band gap of the synthesized nanoparticles is approximately 3.15 eV for ZnO@250, 3.31 eV for ZnO@300, while ZnO@350 was found as 3.17 eV and 3.56 eV. The nanoparticles

were also evaluated for their free radical scavenging property and observed varying antioxidant activities as compared to standard drugs showed higher DPPH scavenging potentials than the various ZnO nanoparticles. The results from DPPH methods revealed that the compounds are capable of donating an electron, consequently, then react with free radicals or terminate chain reactions in a dose-dependent pattern.

### Acknowledgment

The management of Anchor University, Lagos is highly appreciated for the permission to present this work. The Authors are gratefully thankful to the Vaal University of Technology, South Africa where some of the experiments and analyses were carried out.

### References

Alias M, Kassum H, & Shakir C (2014). Synthesis, physical characterization, and biological evaluation of Schiff base M(II) complexes. *Journal of the Association of Arab Universities for Basic and Applied Sciences*. 15: 28-34

Emara A A A, Ali A M, El-Asmy A F, & Ragab E M (2014). Investigation of the oxygen affinity of manganese(II), cobalt(II) and nickel(II) complexes with some tetradentate Schiff bases. *Journal of Saudi Chemical Society*. 18: 762-773.

Ejidike I P (2018). Cu(II) Complexes of 4-[(1E)-N-{2-[(Z)-Benzylidene amino]ethyl}ethanimidoyl]benzene-1,3-diol Schiff base: Synthesis, spectroscopic, *in-vitro* antioxidant, antifungal and antibacterial studies *Molecules*. 23: 1581, 1-18.

Ejidike I P, & Ajibade P A (2015). Transition metal complexes of symmetrical and asymmetrical Schiff bases as antibacterial, antifungal, antioxidant, and anticancer agents: progress and prospects. *Reviews in Inorganic Chemistry*. 35(4): 191-224.

Ejidike I P, & Ajibade P A (2017). Synthesis, spectroscopic, antibacterial and free radical scavenging studies of Cu(II), Ni(II), Zn(II) and Co(II) complexes of 4,4'-{ethane-1,2-diylbis[nitrilo(1E)eth-1-yl-1-ylidene]}dibenzene-1,3-diol Schiff base. *Journal of Pharmaceutical Sciences and Research*. 9(5): 593-600.

Gharibshahi L, Saion E, Gharibshahi E, Shaari A H, & Matori K A (2017). Influence of Poly(vinylpyrrolidone) concentration on properties of silver nanoparticles manufactured by modified thermal treatment method. *PLOS One*. 12(10): e0186094, 1-17.

Gunalan S, Sivaraj R, & Rajendran V (2012). Green synthesized ZnO nanoparticles against bacterial and fungal pathogens. *Progress in Natural Science: Materials International*. 22(6): 693-700.

Kalpanadevi K, Sinduja C R, & Manimekalai R (2013). Characterisation of zinc oxide and cadmium oxide nanostructures obtained from the low temperature thermal decomposition of inorganic precursors. *ISRN Inorganic Chemistry*. 2013(823040): 1-5.

Kulkarni S S, & Shirsat M D. (2015). Optical and structural properties of zinc oxide nanoparticles. *International Journal of Advanced Research in Physical Science*. 2(1): 14-18.

Kumar B, Smita K, Cumbal L, & Debut A. (2014). Green approach for fabrication and applications of zinc oxide nanoparticles. *Bioinorganic Chemistry and Applications*. 2014 (523869): 1-7.

Malathy M, Jayasree R, & Rajavel R (2017). Facile synthesis of CuO nanoparticles from Cu(II) Schiff base complexes: Characterization, antibacterial and anticancer activity. *Smart Science*. 5(2): 100-115.

Meruvu H, Vangalapati M, Chippada S C, & Bammidi S R (2011). Synthesis and characterization of zinc oxide nanoparticles and its antimicrobial activity against *Bacillus subtilis* and *Escherichia coli*. *Rasayan Journal Chemistry*. 4(1): 217-222.

Navale G R, Thripuranthaka M, Late D J, & Shinde S S (2015). Antimicrobial activity of ZnO nanoparticles against pathogenic bacteria and fungi. *JSM Nanotechnology & Nanomedicine*. 3(1): 1033, 1-9.

Xaba, T, Moloto M J, & Moloto N (2016). Bis(2-hydroxyl-1-naphthalenehydrato) metal complexes as source of face-centered-cubic trioctylphosphine oxide-capped ZnO and CdO nanoparticles using Oleylamine as dispersion medium. *Asian Journal of Chemistry*. 28(5): 1015-1020.